AZIMUTHAL VELOCITY ANALYSIS OF 3D SEISMIC FOR FRACTURES: ALTOMENT-BLUEBELL FIELD

Khaled Al Dulaijan and Gary F. Margrave

ABSTRACT

The 3D seismic data was acquired within Bluebell Field, the eastern portion of Altamont-Bluebell field in northeastern Utah. Altamont-Bluebell field is within the Uinta Basin, and is considered an unconventional reservoir in the sense that natural fractures act as fluid storage and conduits in the tight sandstones and carbonates. Information related to fracture orientation and intensity is vital for the development of such reservoirs. Azimuthal variations of P-wave velocities can be a valuable tool for fracture information. Therefore, this paper utilizes Velocity Variations with Azimuth (VVAz) to estimate the direction and intensity of fractured-induced anisotropy within one of the reservoirs, Upper Green River formation.

VVAz inversion method is applied based on the elliptical NMO equation for TI media that was derived by Grechka and Tsvankin (1998). Our code has been tested on a 3D physical modeling dataset and results are shown in another report, Al Dulaijan et. al. (2015). Isotropic NMO velocities are used along with azimuthally variant time residuals to estimate fast and slow NMO velocities and their direction. Hampson-Russell suits VVAz has also been implemented and results are compared in the report.

INTRODUCTION

Bluebell-Altamont field is located in northeastern Utah in the Uinta basin. The Uinta basin is an asymmetric east-west trending basin with a south flank that hat slopes gently. The north flank bounded by east-west trending Uinta Mountains. The Bluebell-Altamont field is located in the northern-central part of the basin (Figure 1). Production is from Tertiary sandstones, shale and carbonates. There are three main targets in the filed: Upper Green River, Lower Green River, and Wasatch (Lynn et. al, 1995). Stratigraphy of the field is shown in Figure 2.

Bluebell-Altamont field is unconventional in the sense that natural fractures act as storage and conduits in the tight sandstones and carbonates. Bluebell field is the eastern portion of the Bluebell-Altamont field. Its accumulative production is 336 MMBO, 588 BCFG, and 701 MMBW. The objective of this study is to identify density and direction of fractures to help in determining well spacing to existing wells needed to effectively drain remaining hydrocarbon reserves in the Bluebell field, and to identify new drilling opportunities (Adams et. al, 2014).

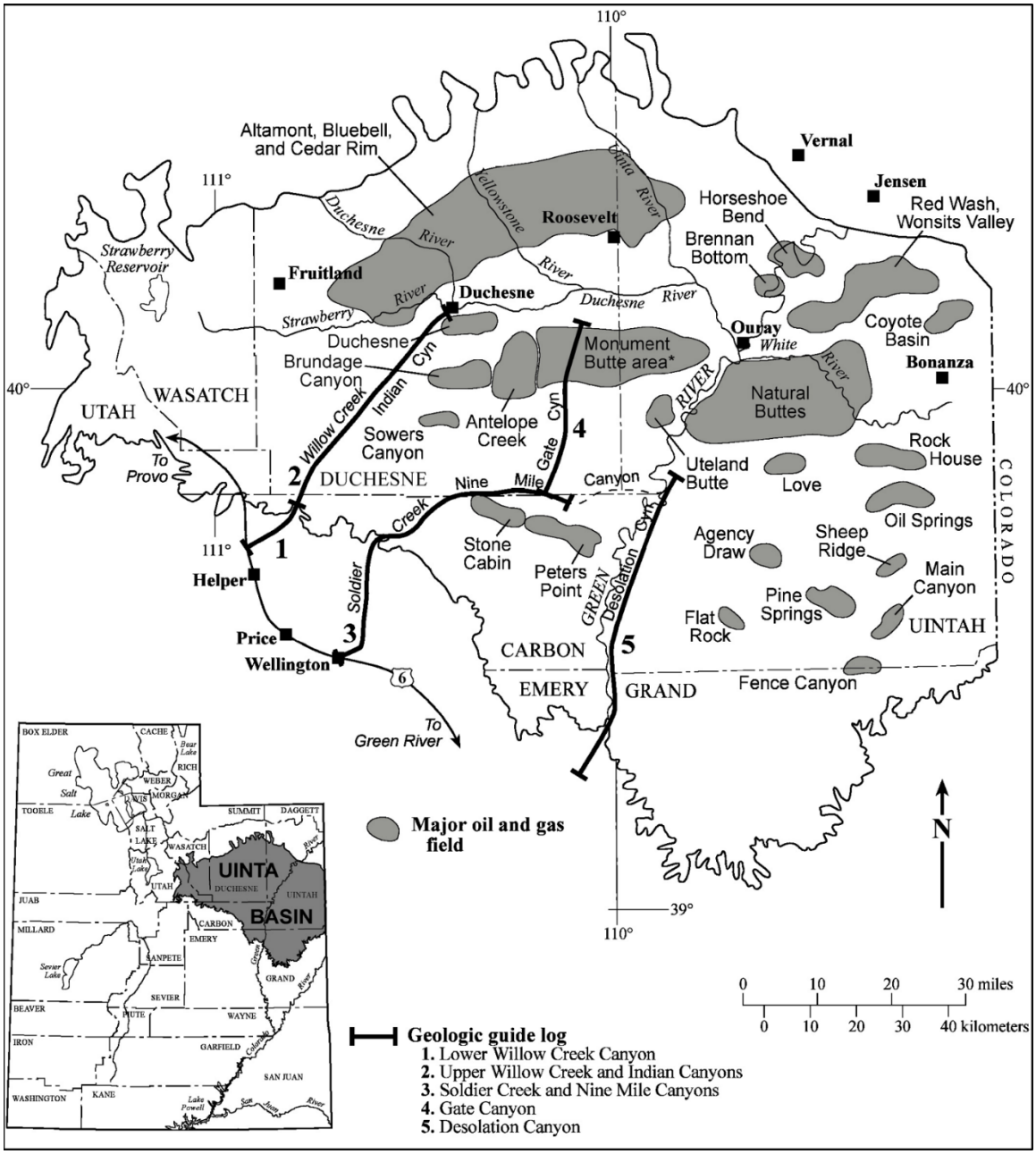

Fig. 1. Location of Uinta basin, Utah (bottom left) and major oil and gas fields within Uinta basin (after Morgan, 2003).

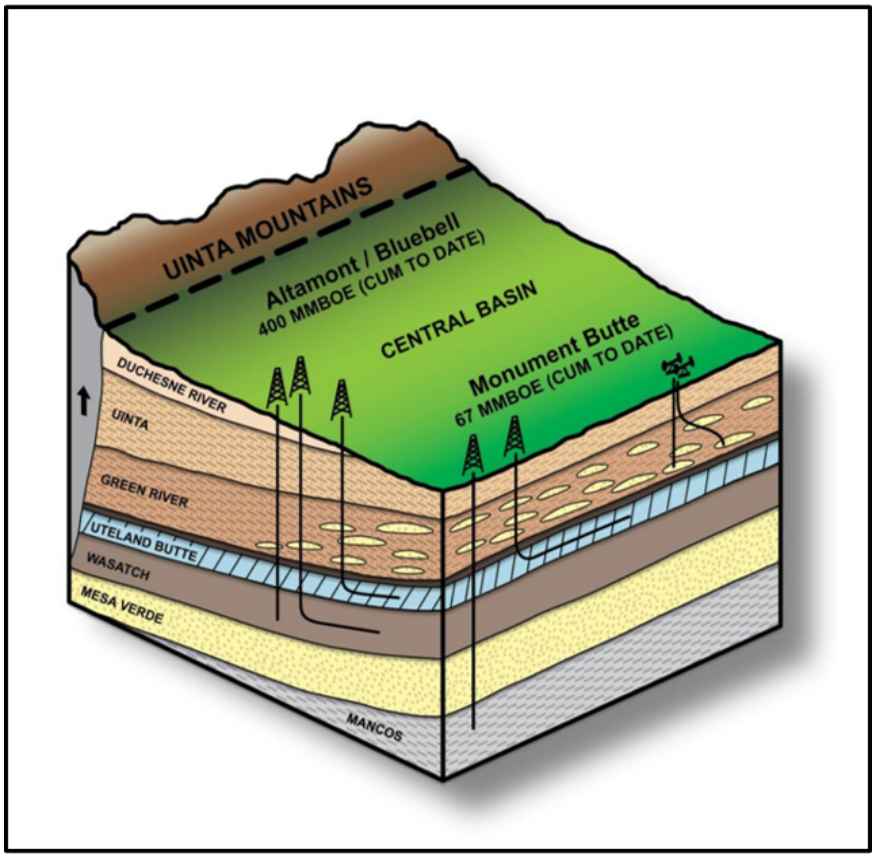

Fig 2. Uinta Basin, Utah. Altamont-Bluebell field is the northern central part of the basin, and Bluebell is the eastern part of Altamont-Bluebell Field. Three main targets are: Upper Green River, Lower Green River (Uteland Butte and Castle Peak), and Wastach formations. Courtesy of: Newfield.

SEISMIC DATA ACQUISTION AND PROCESSING

3D seismic is acquired over an area of 35 square miles within Bluebell field in 2010. Figure 3 shows a basemap of 3D seismic data, with color indicating fold. Two vibrators were used for each shot and an array of six geophones over a 6' circle were used for each channel. The receiver and source intervals are 220'. The receiver lines are oriented E-W and spaced 1100', while source lines are oriented N-S and spaced 660'. Bin size is 110'x110', and the nominal fold is 240. In addition, a zero-offset VSP survey location is indicated by a black circle.

Refraction statics were applied. Heavy noise were observed and suppressed in multiple domains (i.e., shot, CDP, inline-azimuth-shot line). Also, spherical divergence correction, surface-consistent amplitude corrections, and deconvolution were applied. The zero-offset VSP is used to calculate Q that later was accounted for in the 3D seismic data. Isotropic velocity analysis at one-mile interval and NMO corrections were followed by residual statics. Second pass of velocity analysis at half-mile interval were followed by another pass of residual statics. After muting, data is stacked.

Prior to PSTM, data were binned into Common Offset Vector (COV). COV allows azimuthal information to be preserved after PSTM. Isotropic migration is preformed and followed by VTI analysis, and VTI PSTM. PSTM inline stacks intersecting the VSP are shown in Figure 4 with the reference to the base map (bottom right).

SEISMIC DATA ANALYSIS

Top of Upper Green River formation and Mahogany bench are picked and indicated by blue and green respectively on the stacked sections in Figure 4. Upper Green River consists of lacustrine carbonate and clay, while Mahogany bench consists of shale and is a very strong marker (Lucas and Drexler, 1976). Mahogany bench is within the Upper Green River formation. The fracture analysis carried in this paper is on the interval from Upper Green River top to Mahogany bench.

Unlike Amplitude Variations with Azimuth AVAz methods, VVAz methods use base of the target rather than top of the target. The base of the target, the top of Mahogany bench, traveltimes are displayed along the post-stack seismic volume in Figure 5. The Mahogany bench travettimes are shallowest in the northeastern and southwestern part of the survey. Isochron map indicating the thickness of the reservoir from top of Upper Green River to Mahogany Shale is shown in Figure 6. The reservoir thickens at southwest part. At the three main targets, largest incident angles, that can be analyzed, are between 30º to 40º, as shown by Figure 7.

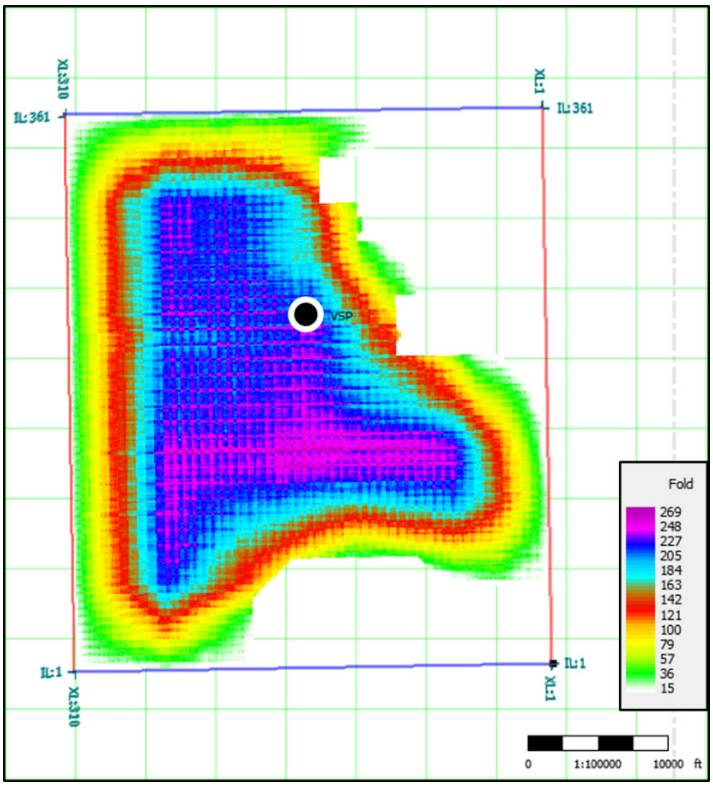

Fig. 3 A basemap of 3D seismic data. Color indicates fold of 110'x110' bins. VSP location is indicated by black circle.

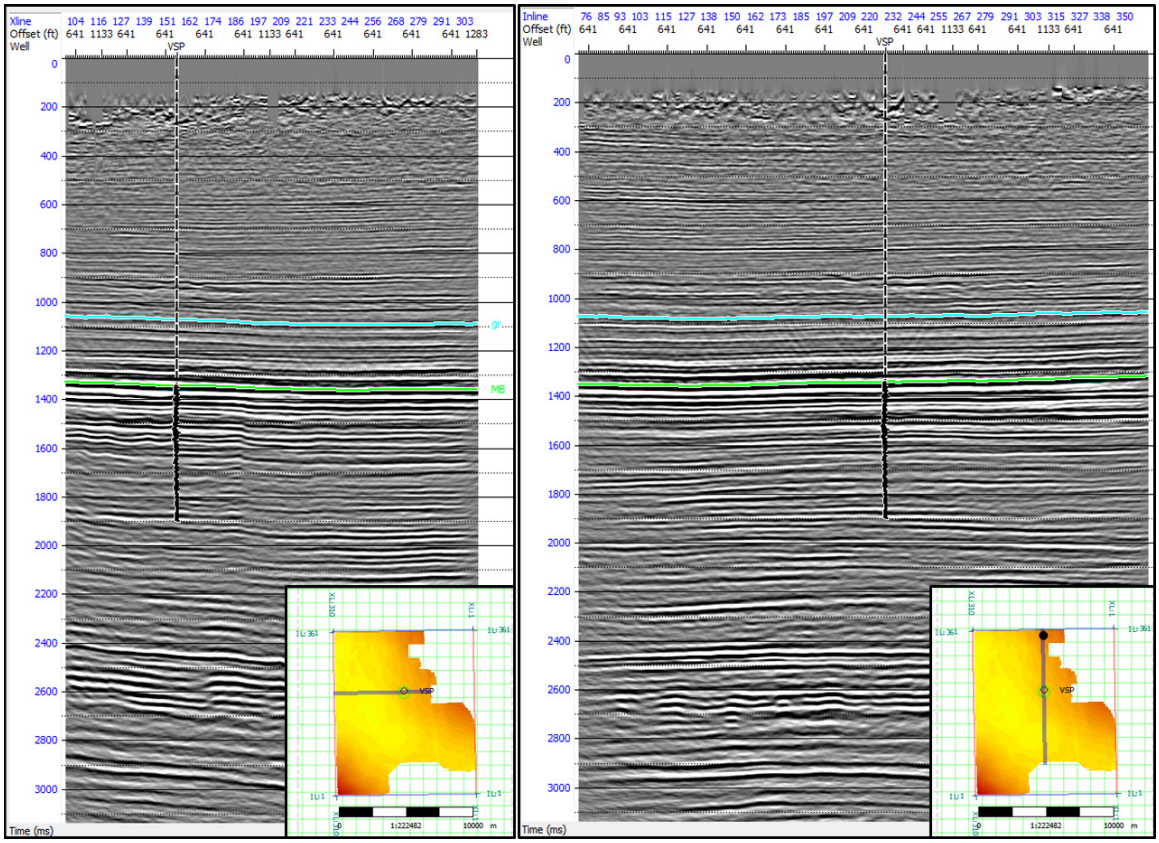

Fig 4. CDP Stack: inline (left) and crossline (right). VSP borehole is indicated in the middle and basemap in the bottom right. Two horizons are indicated Upper Green River (blue) and Mahogany bench (green)

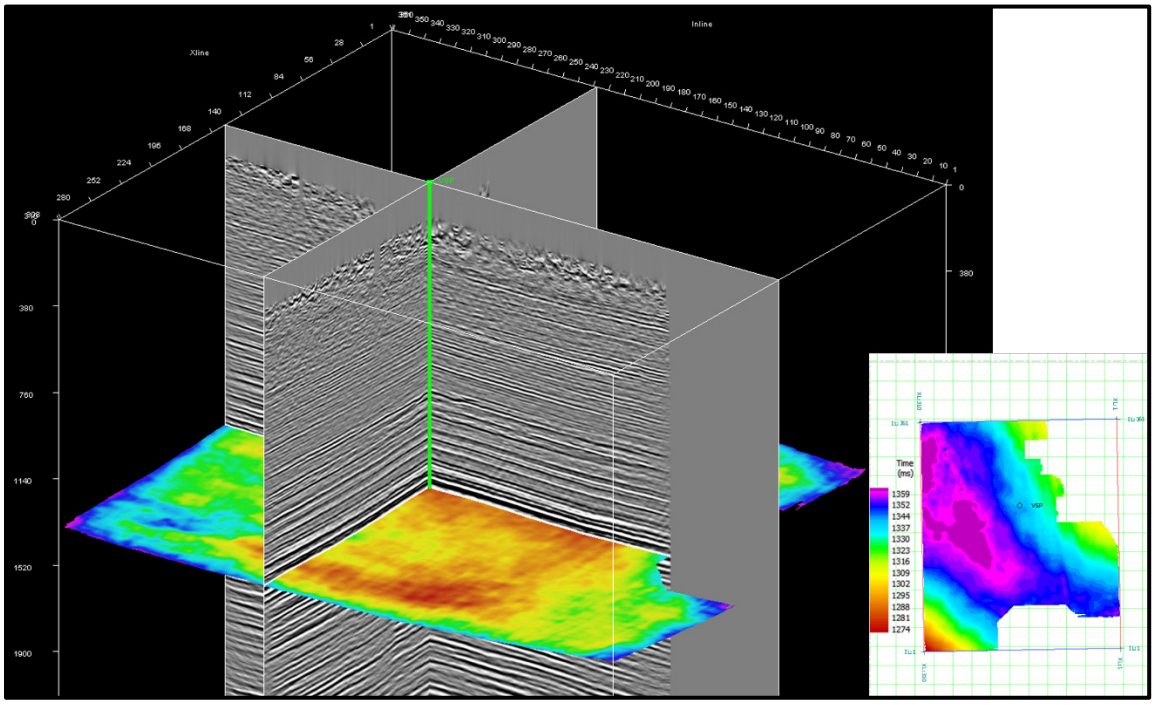

Fig 5. Mahogany bench indicated on seismic volume. Green line indicates VSP.

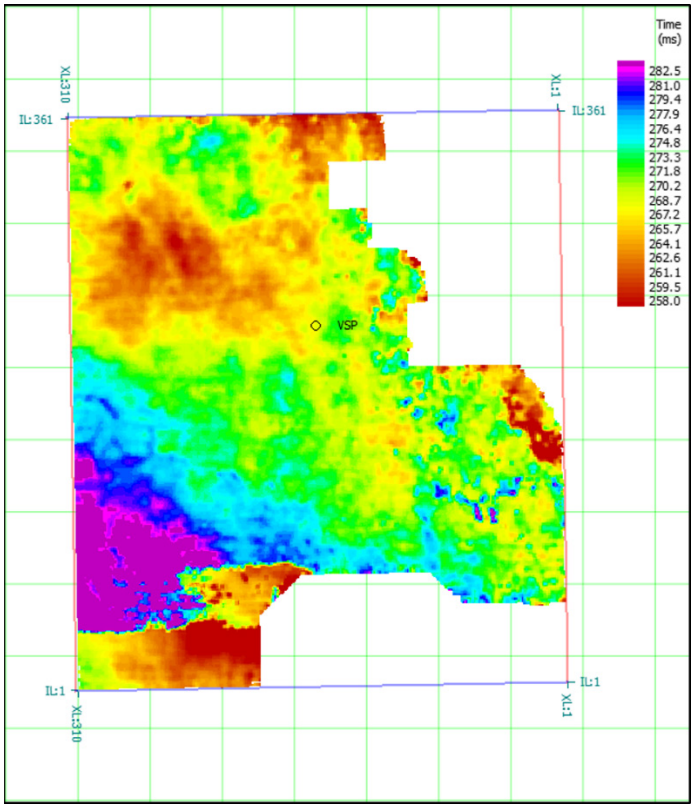

Fig. 6. Isochron indicating the thickness of the reservoir from top of Upper Green River to Mahogany Shale. The reservoir thickens at southwest part.

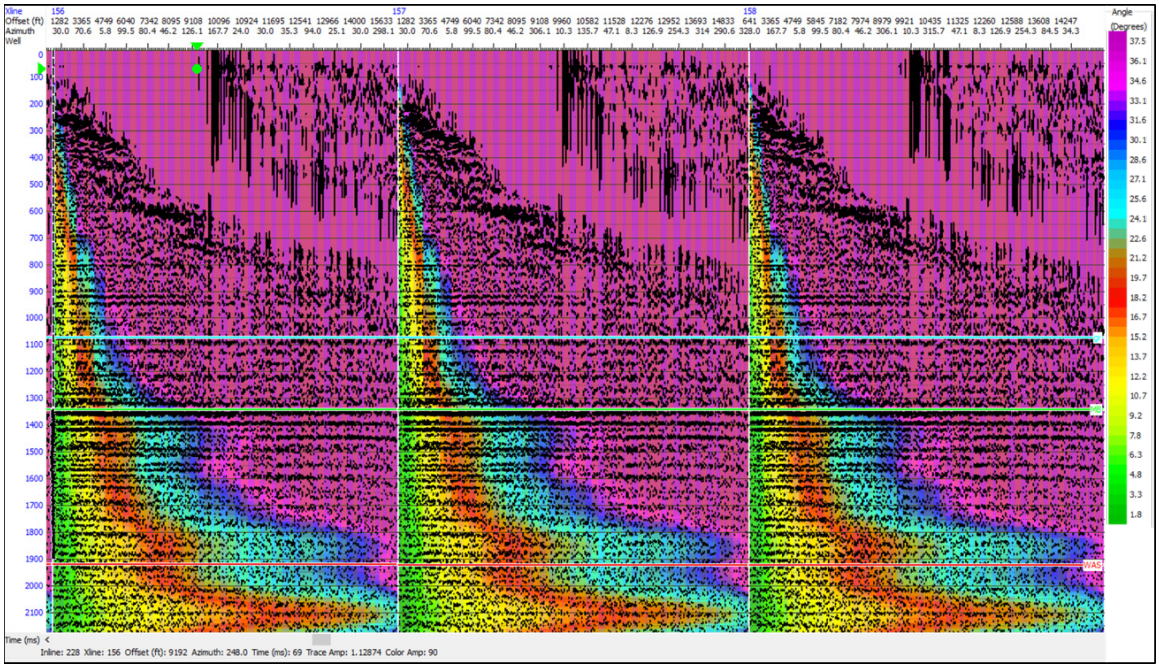

Fig. 7. PSTM image Gather (COV). Color indicates angle of incidences. At target levels, maximum angles are 30° to 40°.

VELOCITY VARIATIONS WITH AZIMUTH

Grechka and Tsvankin (1998) showed that azimuthal variations of NMO velocities can be estimated by an ellipse in the horizontal plane under four assumption. First, the medium is arbitrarily anisotropic and inhomogeneous, so the azimuthal variations in traveltimes are smooth function of surface locations. Second, traveltimes exist at all azimuth. A case of salt domes creating a shadow zone at a specific azimuth violates the second assumption. Third assumption is routinely assumed in seismic data processing steps, such as CMP binning and stacking. That is traveltimes can be described by a Taylor series expansion of $t^2 x_\phi^2$, where t and x_ϕ are traveltimes and source-receiver offset at specific azimuth. Lastly, traveltimes increase with offset at all azimuths. Those assumptions are nonrestrictive in most cases. Grechka and Tsvankin (1998) derived an elliptical NMO equation for TI media where source-receiver offset do no exceed the depth of the reflector. Hyperbolic NMO can be approximated by:

$$T^2 = T_0^2 + \frac{x^2}{V_{NMO}^2(\phi)} \tag{1}$$

, where

$$\frac{1}{V_{NMO}^2(\phi)} = \frac{1}{V_{slow}^2} cos^2(\phi - \beta_s) + \frac{1}{V_{fast}^2} sin^2(\alpha - \beta_s) \tag{2}$$

, where T is the total two-way traveltimes, T_0 is the zero-offset two-way traveltimes. x is the offset, V_{fast} and V_{slow} are the fast and slow NMO velocities respectively. β_s is the azimuth of the slow NMO velocity, while $V_{NMO}(\phi)$ is the NMO velocity as function of the source-receiver azimuth (Figure 8).

Equation (2) can be written as:

$$\frac{1}{V_{NMO}^2(\phi)} = W_{11}\cos^2(\phi) + 2W_{12}\cos(\phi)\sin(\phi) + W_{12}\sin^2(\phi) \tag{3}$$

, where W_{11}, W_{12}, and W_{22} are the ellipse coefficients that are related to the slow and fast NMO velocities and to the azimuth of the slow NMO velocity by

$$\frac{1}{V_{fast}^2} = \frac{1}{2}[W_{11} + W_{22} - \sqrt{(W_{11} - W_{22})^2 + 4W_{12}^2} \tag{4}$$

$$\frac{1}{V_{slow}^2} = \frac{1}{2}[W_{11} + W_{22} + \sqrt{(W_{11} - W_{22})^2 + 4W_{12}^2} \tag{5}$$

$$\beta_s = \tan^{-1}\frac{W_{11} - W_{22} + \sqrt{(W_{11} - W_{22})^2 + 4W_{12}^2}}{2W_{12}} \tag{6}$$

The azimuth of the fast velocity is 90° away from the azimuth of the slow velocities as shown by Figure 8 (Jenner, 2001). The total travel can be written as:

$$T^2 = T_0^2 + x^2 \cos^2(\phi) W_{11} + 2x\, cos(\phi)\sin(\phi) W_{12} + x^2 \sin^2(\phi) W_{22}. \quad (7)$$

Equation (7) can be written as:

$$d = Gm\,,$$

where d is n-dimensional data vector, m is the 6-dimensionl model parameter vector, and G is the n-by-4 data kernel as:

$$\begin{pmatrix} T_1^2 \\ T_2^2 \\ \vdots \\ T_n^2 \end{pmatrix} = \begin{pmatrix} 1 & x_1^2 \cos^2(\phi_1) & 2x_1\, cos(\phi_1)\sin(\phi_1) & x_1^2 \sin^2(\phi_1) \\ 1 & x_1^2 \cos^2(\phi_1) & 2x_1\, cos(\phi_1)\sin(\phi_1) & x_1^2 \sin^2(\phi_1) \\ \vdots & \vdots & \vdots & \vdots \\ 1 & x_{n1}^2 \cos^2(\phi_n) & 2x_1\, cos(\phi_1)\sin(\phi_1) & x_1^2 \sin^2(\phi_1) \end{pmatrix} \begin{pmatrix} T_0^2 \\ W_{11} \\ W_{12} \\ W_{22} \end{pmatrix}. \quad (8)$$

Isotropic NMO velocities V_{NMO} and zero-offset traveltimes T_0 are used along with azimuthally variant time residuals, dT_ϕ to estimate azimuthal traveltimes, T, as follows:

$$T = T_x + dT_\phi \quad (9)$$

, where

$$T_x = \sqrt{T_0^2 + \frac{x^2}{V_{NMO}\text{^}2}} \quad (10)$$

The azimuthally-variant residuals were auto-picked and applied to the COV gathers. Figure 9 shows the gathers before applying the residual traveltimes (left) and after applying them (right). A sequence of white and yellow backgrounds indicate offset. Offset changes where background color changes. The Mahogany bench time picks from stacked data is indicated by light green on the pre-stack COV gather. It can be seen that the flatness of Mahogany bench is significantly improved after the application residual travel times, especially at larger offsets.

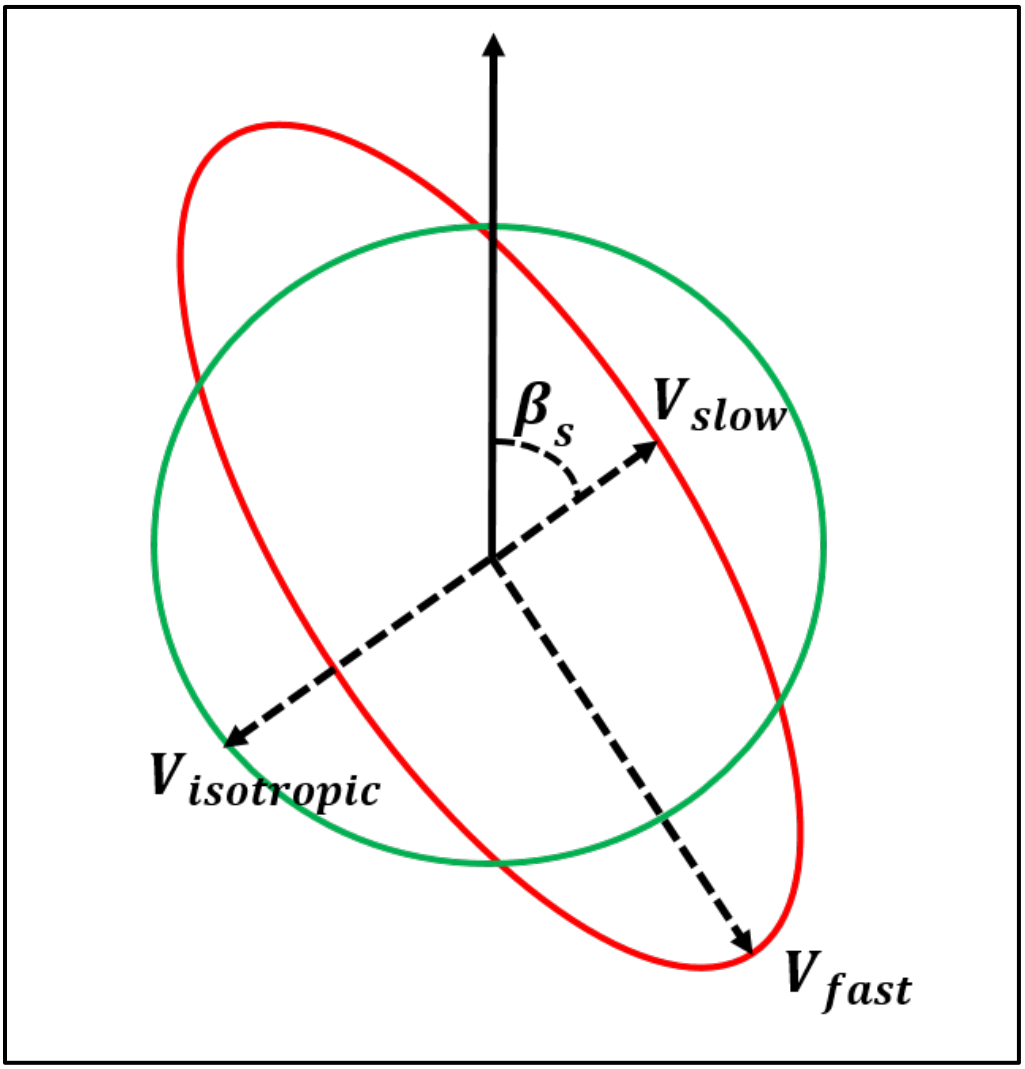

Fig. 8. Isotropic RMS velocity vs azimuthally variant RMS velocity.

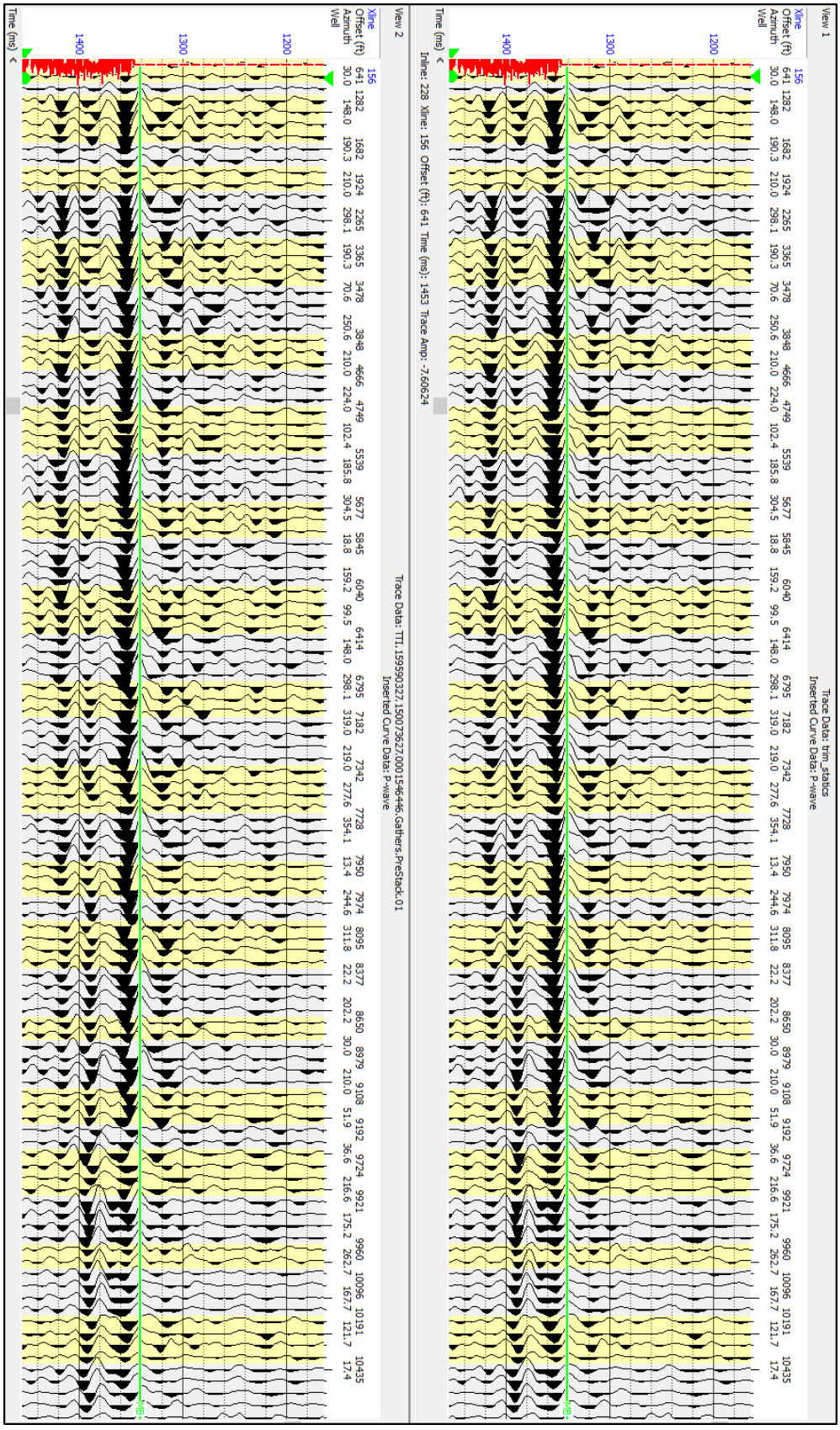

Fig 9. COV Gathers: Before (left) and after (right) applying azimuthal residuals.

RESULTS

VVAz inversion has been performed in Matlab as described above to the part of the Mahogany Bench around the VSP. Fast RMS velocity, slow RMS velocity, and their directions were calculated. Figure 10 compares isotropic RMS velocity to fast and slow RMS velocities. Coordinates are with reference to the VSP borehole. From those three velocities, a velocity anisotropy percentage was calculated by dividing the difference between the fast and slow RMS velocities by the isotropic RMS velocity. Besides the method described above, VVAz was performed in Hampson-Russell Suites, and the results are compared.

Figures 11, 12 and 13 compare the percentage and direction of anisotropy obtained by our code to Hampson-Russell's. We can see that anisotropy percentage obtained by both methods go up to less than 1.5%. Higher anisotropy zones, in both maps, are observed in northeast and southwest. In Figure 12, it can be seen that anisotropy orientation, obtained by methods, falls in the same quadrant. Figure 13 is a zoomed-in version of Figure 12 with selected area from Hampson-Russell's and their corresponding area from our method. Arrows on left map from top to bottom have values of 40º, 19º, and 43º from *x*-axis.

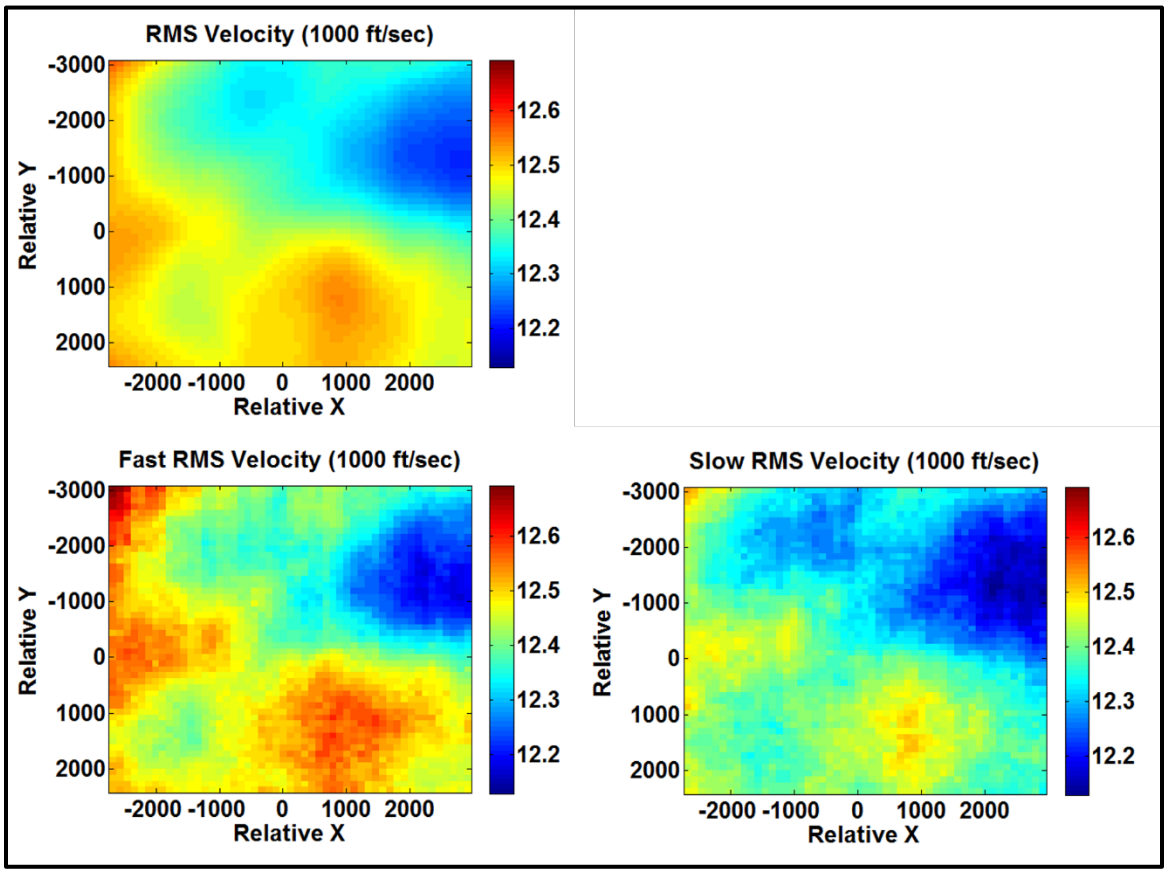

Fig. 10. Isotropic RMS velocity vs. fast RMS velocity vs. slow RMS velocity in (1000 ft/s).

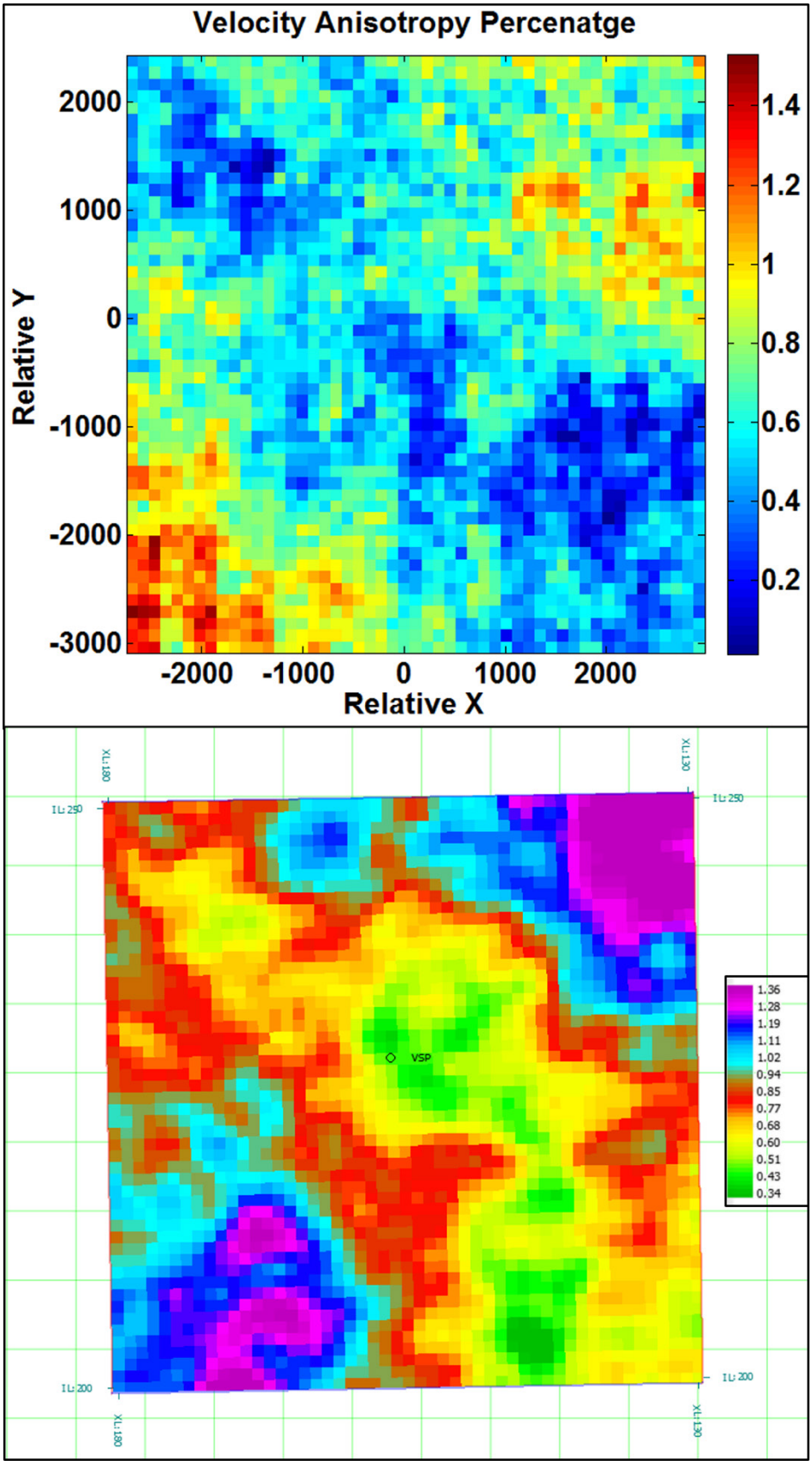

Fig 11. Comparison of anisotropy percentage obtained by two methods.

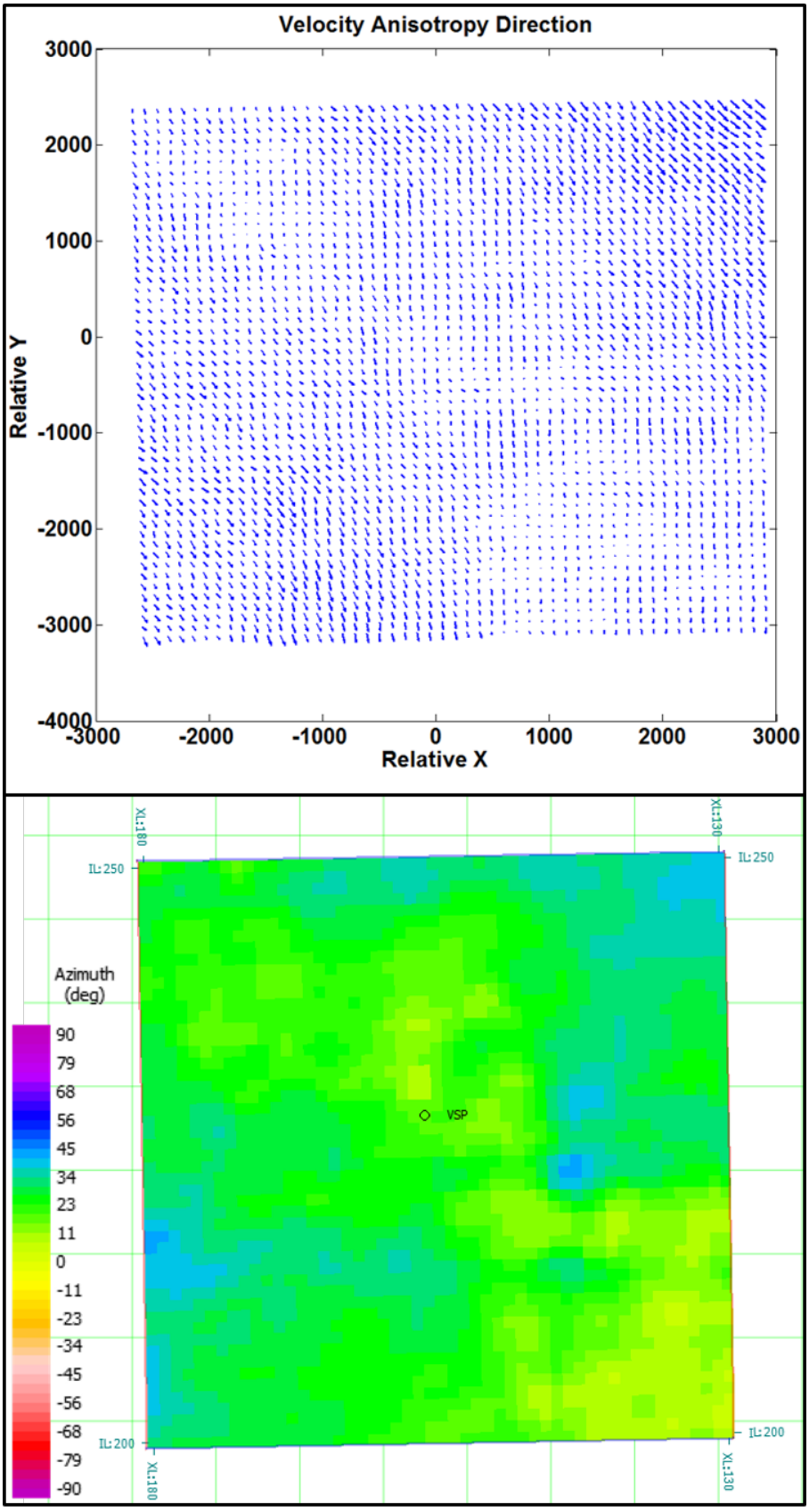

Fig 12. Direction of VVAz by two methods.

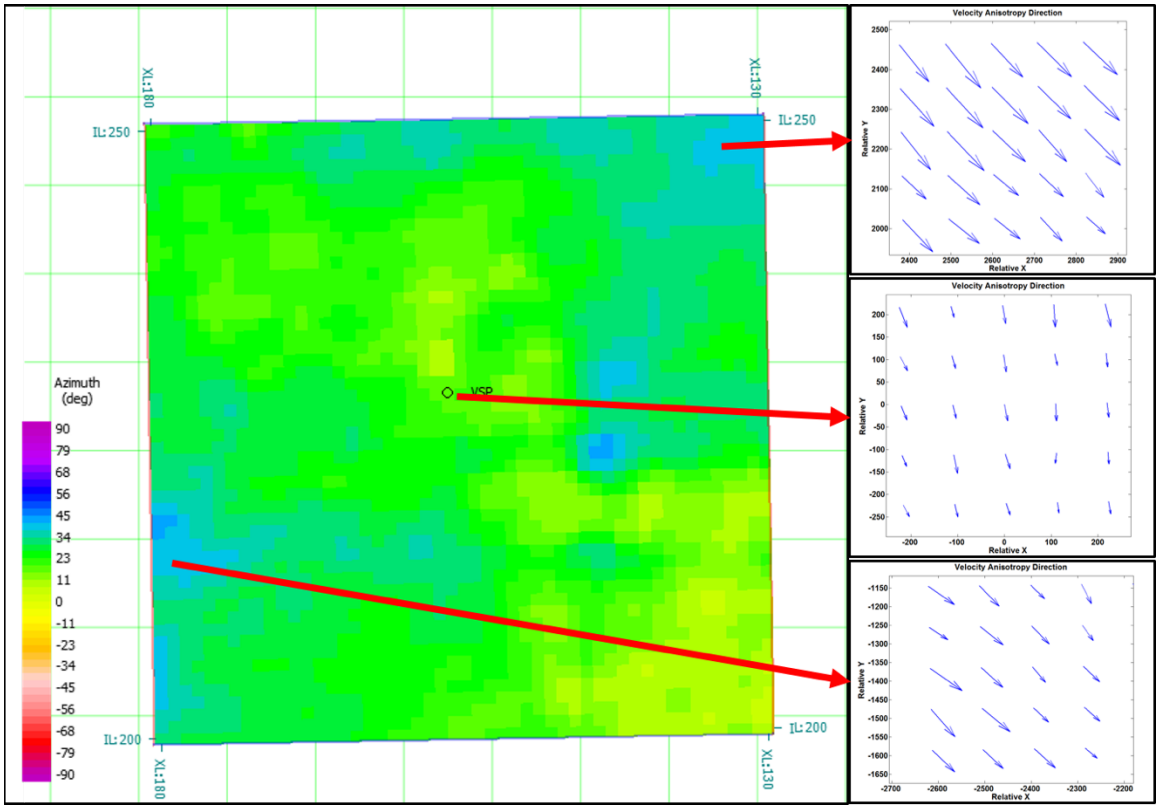

Fig 13. Comparison of two methods of VVAz. Color on left map indicates angle of fast velocity from the x-axis. Arrows on left map from top to bottom have values of 40º, 19º, and 43º from *x*-axis.

CONCLUSIONS AND FUTURE WORK

For the development of unconventional reservoirs, azimuthal variations of P-wave velocities can be a valuable tool for fracture information. In this paper, we have implemented an AVAz workflow to 3D pre-stack seismic data from Altamont-Bluebell field. Our target was the shallowest from the three targets of Uinta Basin, Upper Green River to Mahogany Bench. Maps of anisotropy intensity and direction were obtained and compared to maps that we obtained using Hampson-Russell Suites. Both direction and intensity maps correlate well in both models.

We think that the use of interval velocity has an advantage over the use of RMS velocities because it will make VVAz less sensitive to overburden properties. Therefore, we plan to improve our code by using a Dix-type formula to obtain interval NMO ellipses (Grechka et al., 1999) We plan to further investigate velocity variations with azimuth (HTI anisotropy) and velocity variations with offset (VTI), in order to relate results to vertical fractures and horizontal fractures. Also, we plan to perform post-stack analysis on the data to estimate intense zones of fractures and the direction. Further pre-stack analysis of the data is going to be applied, including geomechanical driven attributes obtained by pre-stack elastic inversion to estimate brittle zones of the reservoir. The pre-stack data will be analyzed for Amplitude Variations with Azimuth AVAz using Rüger (2001) and Fourier

coefficients to estimate fractures intensity and directions maps. Fractures maps obtained from different methods will be compared and related to production data.

ACKNOWLEDGMENT

We thank the sponsors of CREWES for their support. We also gratefully acknowledge support from NSERC (Natural Science and Engineering Research Council of Canada) through the grant CRDPJ 379744-08. Also, we are grateful to Devon Energy for permission to use the data and publish the results. We thank CGGVeritas for the use of Hampson-Russell software. The first author would like to thank Khaled Almuteri for proofreading the report and useful discussions, and Dr. Jon Downton Hampson-Russell ProAz workshop and for useful discussion. Also, he would like to thank Saudi Aramco for graduate study sponsorship.

REFERENCES

Adams, C., 2014, Ministry of Natural Gas Development: Northeast BC Activity Update.

Al Dulaijan, K., G. Margrave and J. Wong, 2015, 3D seismic physical modeling for azimuthal variations of P-wave velocity: CREWES Research Report.

CGGVeritas, 2014, Hamson-Rusell Software Manual: Release 9.

Grechka, V., & Tsvankin, I., 1998, 3-D description of normal moveout in anisotropic inhomogeneous media. Geophysics, 63(3), 1079-1092.

Jenner, E., 2001, Azimuthal anisotropy of 3-D compressional wave seismic data, Weyburn Field, Saskatchewan, Canada: Ph.D. thesis, Colorado School of Mines.

Lucas, P. T., & Drexler, J. M.,1976, Altamont-Bluebell--a major, naturally fractured stratigraphic trap, Uinta basin, Utah.

Lynn, H. B., Bates, R., Layman, M., & Jones, M. ,1995, Natural fracture characterization using P-wave reflection seismic data, VSP, borehole imaging logs, and the in-situ stress field determination. In Low Permeability Reservoirs Symposium. Society of Petroleum Engineers.

Morgan, C. D., 2003, Geologic Guide and Road Logs of the Willow Creek, Indian, Soldier Creek, Nine Mile, Gate, and Desolation Canyons, Uinta Basin, Utah (OFR-407).

Rüger, A., 2001, Reflection coefficients and azimuthal AVO analysis in anisotropic media. Society of Exploration Geophysicists.